

Fig. 1. Piezosensor surrounded with expanded metal (a) and cross section of the active composite (b).

casting. Zn-coated inserts are embedded into thin-walled components. The influence of the thickness of the zinc layer on both the formation of the interface zone and the mechanical properties of the compound is investigated.

2. Experimental procedures

The insert employed is an expanded metal consisting of Al99.5. The meshes have a length of 10 mm and a width of 5 mm. The cross section of the strands is 1.5 mm × 1 mm, the thickness is 2.5 mm. Samples with a dimension of 100 mm × 30 mm are prepared for the compound casting experiments.

2.1. Coatings

A pre-treatment of the insert's surface before coating is essential for a sufficient layer adhesion. Firstly, the surface of the structure is sandblasted to provide a uniform surface and to remove sharp edges. Secondly, it is etched in a sodium hydroxide solution (100 g l^{-1} NaOH, 75°C , 50 s) to remove the surface layer containing oxides and remaining lubricants. After finishing the pre-treatment a zincate treatment is performed to deposit a zinc layer on the surface. The zincate treatment is an established coating method, usually applied as a pre-treatment for aluminium surfaces prior to electrodeposition as reported [6]. It is a currentless immersion process with a solution containing 450 g l^{-1} NaOH and 50 g l^{-1} ZnO. Wernick et al. [7] have shown that this is a suitable solution composition for a successful zincate treatment. The procedure includes two parallel chemical reactions. On the one hand, the alkaline solution, containing NaOH and Zn anions, removes the Al_2O_3 layer by etching. On the other hand, a redox reaction proceeds, where Al oxidizes and dissolves and Zn anions are reduced and deposited. The result is a thin metallic Zn-layer. The layer thickness is between 100 nm and 500 nm, because the reaction stops as soon as the surface is completely covered with Zn and the ion-exchange reaction has no driving force anymore.

Zinc electroplating is performed with an electrolytic cell to achieve thicker Zn-layers. The electrolyte for this additional coating process contains 150 g l^{-1} ZnSO_4 , 50 g l^{-1} $\text{N}_2\text{H}_8\text{SO}_4$ and 15 g l^{-1} boric acid. The parameters for the Zn deposition are current density (2.5 A dm^{-2}) and bath temperature (35°C). The desired layer thickness is adjusted by the coating time and controlled by weighing the specimens as well as optical microscopy. The layer thickness is varied in 5 steps between $2 \mu\text{m}$ and $22 \mu\text{m}$ for the casting experiments.

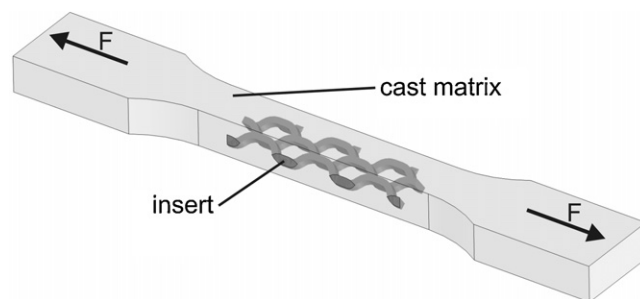


Fig. 2. Schematic illustration of the specimen with integrated insert for the tensile tests.

2.2. Compound fabrication

A FRECH die casting unit DAK 450/54 with a locking force of 450 tons is used for the fabrication of the compounds. In addition, a FONDAREX vacuum device is applied to the mould in order to generate a low pressure during mould filling. Thus, gas porosity and pore sizes in die castings can be reduced as demonstrated [8]. Components with the dimension $178 \text{ mm} \times 178 \text{ mm} \times 5 \text{ mm}$ are produced. During each die casting cycle one layer of pre-treated expanded metal is placed inside the cavity before mould closure. All experiments are performed using the standard aluminium casting alloy 226D (AlSi9Cu3(Fe)) at a mould temperature of 220°C .

2.3. Characterisation

Half of the castings is cut and polished to analyse both microstructure and element composition at the interfacial region and to obtain a smooth surface for microhardness testing. The microstructure is investigated applying both optical microscopy and scanning electron microscopy (SEM Philips XL30). The EDX system of the SEM and the microprobe Jeol JXA 8100 are used for analysing the element composition. The microhardness measurements are performed with a Leco M-400-G hardness tester using a Vickers indenter at a load of 10 g and a dwell time of 10 s.

The other half of the compound castings is machined to prepare samples for tensile testing. Eight samples per initial layer thickness are prepared. The geometry of the samples is based on the standard DIN 50125. A schematic drawing of a specimen with integrated insert is shown in Fig. 2. The tensile tests are performed with the tensile testing machine Instron 4505 Retrofit. The samples are loaded with 2 MPa s^{-1} , the elongation is measured with an extensometer. Yield strength, tensile strength and elongation at fracture are relevant parameters for the evaluation of the compound.

3. Results and discussion

3.1. Coatings

A thin zinc layer is deposited on the surface of the expanded metal after the zincate treatment. Fig. 3 shows a SEM image of the zincate-treated surface. It is almost completely covered with a continuous Zn layer. The honeycomb-like indentations are a result of sandblasting prior to coating. Just a few small uncoated sections are visible and indicated in Fig. 3. Impurities like remaining lubricants on the structure's surface might inhibit the intended reactions during the zincate treatment there. However, the fraction of uncoated surface is too small to influence the results of the compound casting process. Furthermore, these sections are covered with zinc during the following electrochemical deposition.

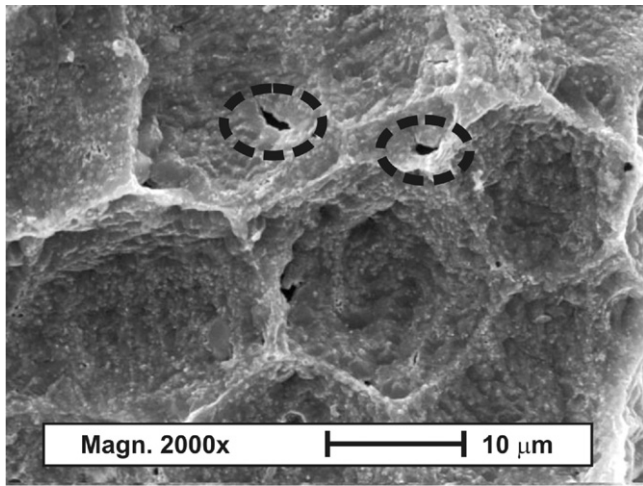


Fig. 3. SEM micrograph of the zincate-treated insert surface. Uncoated areas are indicated.

The additional zinc coating deposited via galvanizing is shown in Fig. 4. The morphology of the coating does not depend on its thickness, which is adjusted over coating time at constant current density. The layer thickness increases linearly with time. However, the rough surface of the insert caused by sandblasting is the reason for minor variations of the layer thickness.

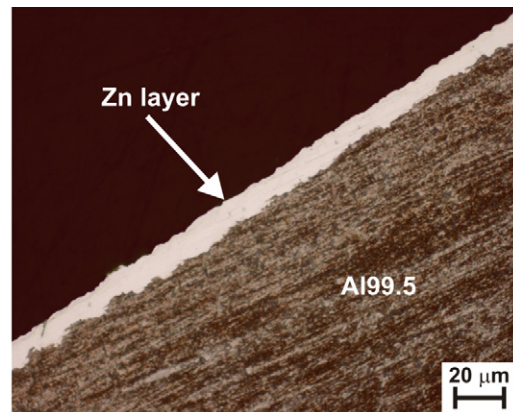
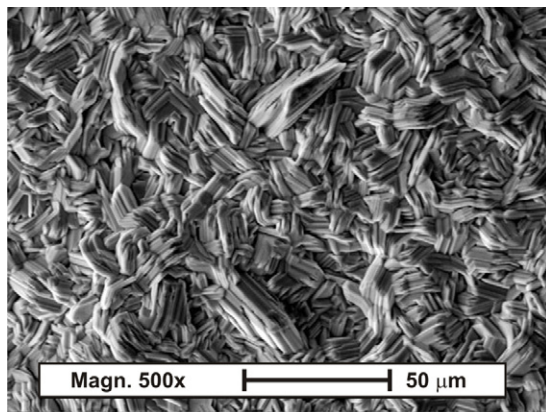


Fig. 4. SEM micrograph of the insert surface coated with Zn and optical microscopy image of the cross section of a sample after electrochemical Zn deposition. The layer thickness is about 12 μm.

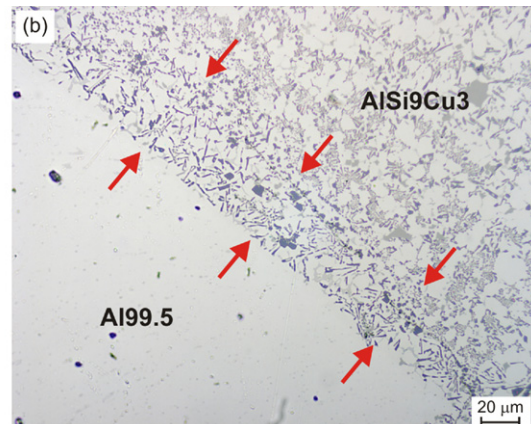
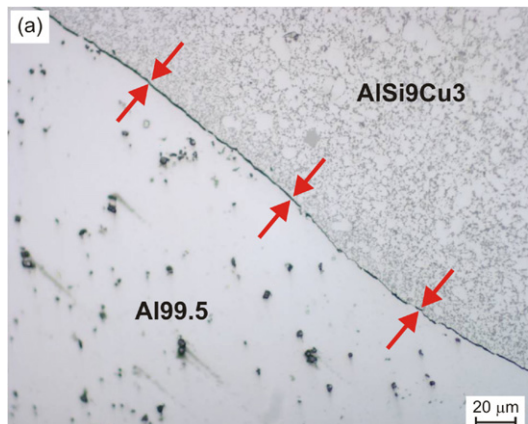


Fig. 5. Micrographs showing the transition zone from the insert to the matrix. A gap forms with zincate treated Al99.5 (a). A continuous metallic transition can be achieved with zincate treated + additionally Zn coated Al99.5 (b).

3.2. Interface formation

The thin Zn coating deposited only by zincate treatment is insufficient to produce a sound metallic bonding. A gap occurs between the insert and the cast matrix (Fig. 5a). The Zn coated structure is exposed to elevated temperatures of about 220 °C for 20 s inside the mould before it is filled. Presumably, diffusion processes of the very thin Zn-layer into the solid aluminium are activated during this time, which further enables surface reactions, e.g. reoxidation. The surface activation is not longer sustained and no metallic bonding occurs.

The desired metallic bonding can be achieved with thicker Zn-layers deposited via galvanizing. A micrograph of the cast compound shows the formation of a continuous metallic transition from the single phase Al99.5 to the partially eutectic Al-alloy AlSi9Cu3 (Fig. 5b).

Thickness and composition of the transition zone vary with different initial Zn layer thicknesses. The transition zone can be divided into three different zones defined by the zinc concentration, see Fig. 6. During fabrication, the Zn layer transforms into three zones: a diffusion zone into the insert, a Zn-rich interlayer and a diffusion zone into the cast matrix.

EDX linescans through the transition zone between Al99.5 and the cast alloy for initial layer thicknesses of 6 and 22 μm are presented in Fig. 7. Further alloying elements of the cast alloy like copper or iron are neglected in the plots as their concentration is below 3 wt% (Cu) and 1 wt% (Fe), respectively. The three zones of the transition zone can be identified for different initial layer thicknesses.

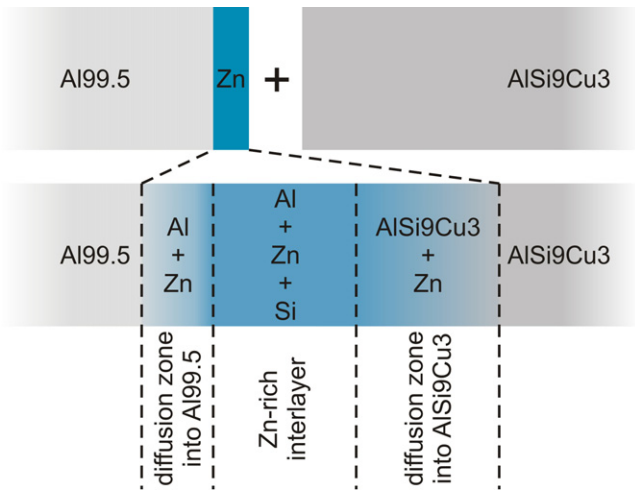


Fig. 6. Schematic illustration of the variation of the zinc distribution during the casting process.

Starting from Al99.5, the first zone is the diffusion zone into Al99.5, where zinc diffuses into the solid insert. Fig. 8 shows a linescan through this diffusion zone, detected with the microprobe with a spot size of 1 μm for a more accurate resolution. Following Fick's 2nd law of diffusion, the zinc concentration profile correlates with typical diffusion profiles into solid bodies. This diffusion process takes place until the component is cooled down to room temperature.

The next zone is the Zn-rich interlayer with nearly constant zinc concentration. The microstructure of this interlayer is shown in Fig. 9. The ternary system Al–Si–Zn is formed. The main component of the microstructure is supersaturated Al solid solution. More zinc

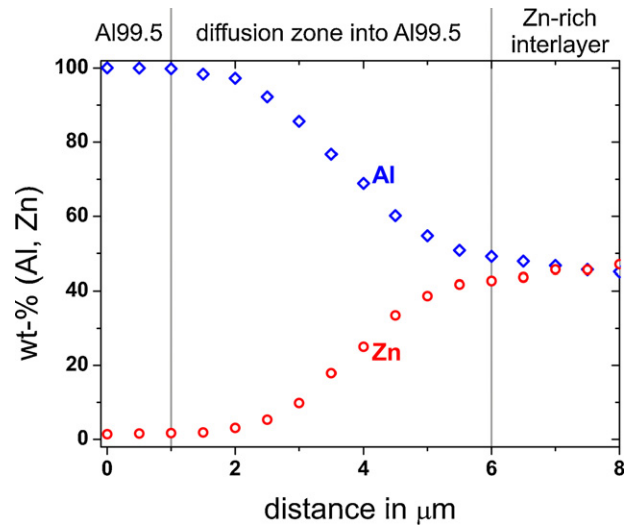


Fig. 8. WDX linescan across the diffusion zone into Al99.5 for an initial zinc layer thickness of 22 μm .

is dissolved in the Al solid solution compared to the cast matrix. This results in a brighter contrast of this phase in the SEM image. In addition, silicon precipitates can be identified in the zone. These precipitates are plate-type and thus needle-shaped in the cross section. The third phase is a ternary eutectic in the interdendritic area with zinc, Al solid solution and silicon. The zinc concentration is very high there. Consequently, it appears very bright in the SEM image.

Jacobs and Spencer [9] have published a calculated isopleth of the ternary system Al–Si–Zn at 4.7 at% Si including a comparison with experimental results. They have pointed out that for each

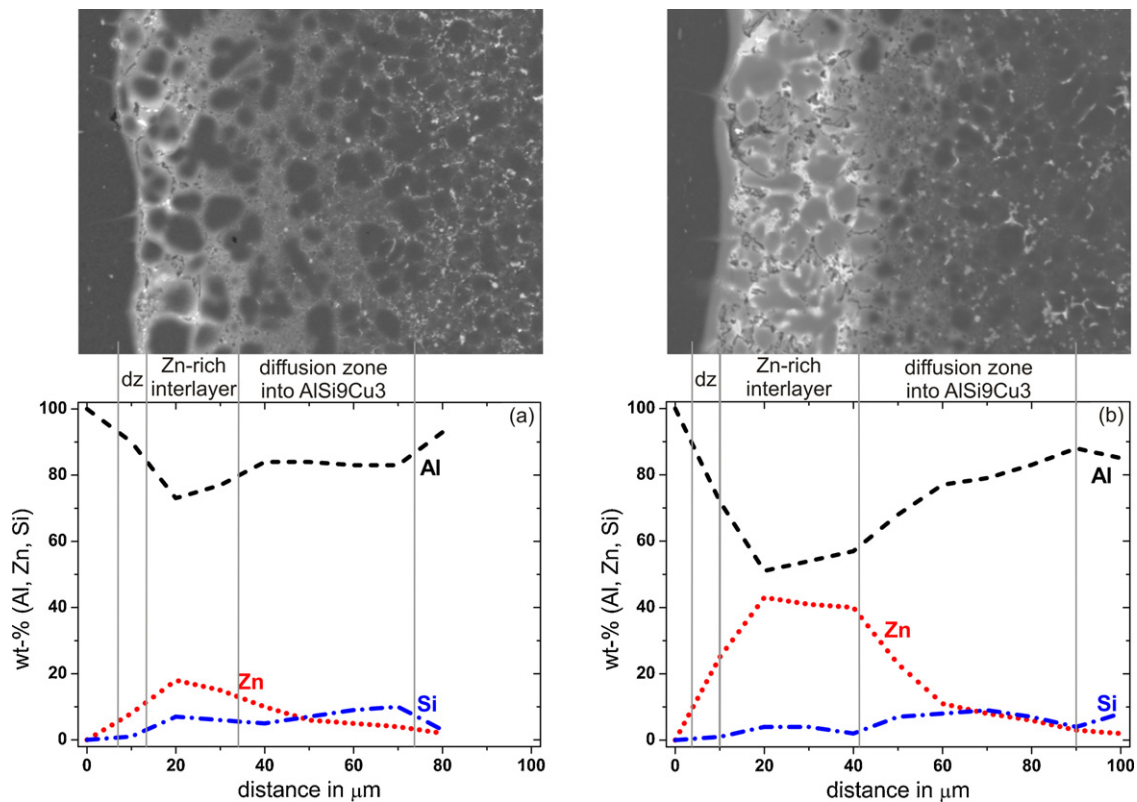


Fig. 7. EDX concentration profiles across the transition zone for an initial layer thickness of 6 μm (a) and 22 μm (b). The diffusion zone into Al99.5 (dz) cannot be shown in detail with EDX.

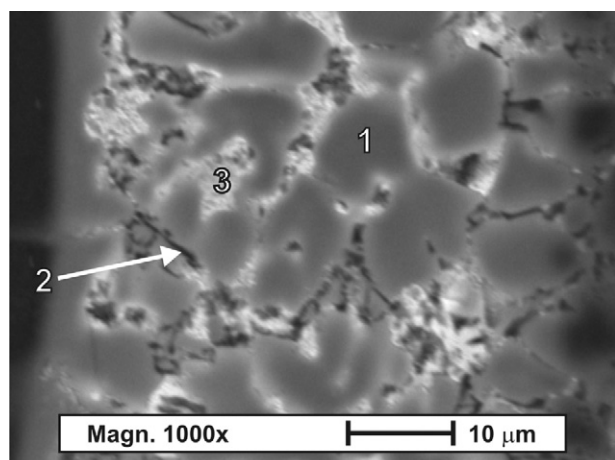


Fig. 9. Microstructure of the Zn-rich interlayer with Al solid solution (1), Si precipitates (2) and ternary eutectic (3). The initial layer thickness was 22 μm .

phase of the ternary system Al–Si–Zn, the physical interactions between the elements Al, Si and Zn can be explained by a summation of the binary interactions of the elements only. Hence, the ternary interaction of the three elements can be neglected in the thermodynamic description of Al–Si–Zn alloys.

Massalski et al. [10] have published the three relevant binary phase diagrams Al–Si, Al–Zn and Si–Zn. All combinations are eutectic systems.

The binary alloy Al–Si is well known for processing in die casting. It is a eutectic system with solid solubility of Si in Al solid solution. The microstructure at room temperature consists of primary Al solid solution and Si + Al solid solution eutectic.

An important criterion of the binary alloy Al–Zn is the decrease of the solid solubility of Zn in Al with decreasing temperature. The solid solubility is more than 80 wt% at a temperature of 400 $^{\circ}\text{C}$ whereas the solubility is just round about 1 wt% at room temperature. Saray and Purcek [11] have recently explained the microstructure of an as-cast Al–40 wt% Zn alloy with dendritic Al solid solution which is surrounded by Zn-rich Al+Zn eutectoid region in the interdendritic area.

The binary alloy Si–Zn is a system without solid solubility. Si and Zn grains form the microstructure at room temperature.

The microstructure of the Zn-rich interlayer is a consequence of these three relevant binary phase diagrams and the isopleth of the ternary system Al–Si–Zn at 4.7 at% Si. However, it is important to consider, that the phase diagrams are valid for equilibrium solidification. For processes like high pressure die casting with very high cooling rates, the validity is limited.

Both width and zinc concentration of this part of the transition zone vary with different initial layer thicknesses. The fraction of ternary eutectic as well as the Zn content in the Al solid solution decreases with decreasing initial layer thickness. This illustrates the darker contrast in the SEM image (Fig. 7).

Zinc keeps completely dissolved in the solid solution and no ternary eutectic appears if the zinc content is below the solid solubility in aluminium for these cooling conditions. However, this effect occurs for initial layer thicknesses below 6 μm .

The third part of the transition zone is the diffusion zone into the cast matrix. The zinc content decreases with increasing distance to the interfacial region.

3.3. Microhardness

The hardness profiles measured across the transition zone for initial layer thicknesses of 6 and 22 μm are plotted in Fig. 10. Start-

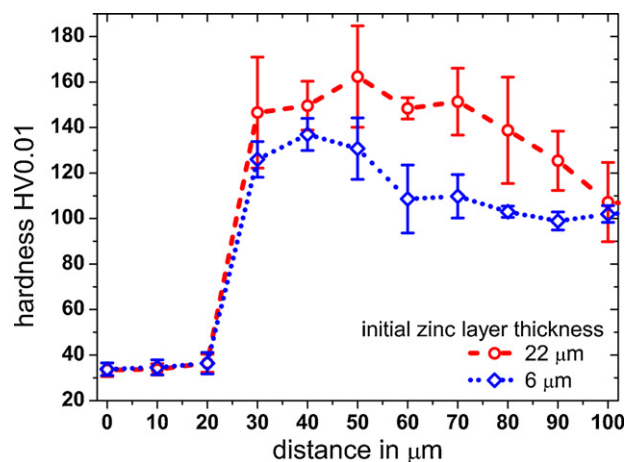


Fig. 10. Microhardness profiles across the transition zone for different initial layer thicknesses.

ing point of the profiles is always the Al99.5 insert with a hardness of 35–40 HV. The hardness increases to 160 HV across the Zn-rich interlayer and decreases across the diffusion zone into AlSi9Cu3 to 100 HV.

The crucial difference between the transition zone and the cast matrix is the zinc content. Tavoosi et al. [12] have demonstrated the effect of the alloying element zinc in aluminium powder particles by mechanical alloying. Zinc causes an increase of hardness due to solid solution hardening. This hardening effect is enhanced with increasing zinc content in bulk materials as demonstrated [13]. Consequently, the remaining zinc in the Al solid solution in the transition zone causes the hardness increase. This is the reason for the good correlation between the zinc concentration profiles and the hardness profiles, also for different initial layer thicknesses.

3.4. Mechanical properties

The considerations of the mechanical properties are divided into elastic and plastic behaviour. The elastic deformability is characterised by the yield strength. This property is plotted against the initial layer thickness in Fig. 11. Evidently, the integration of the insert does not influence the yield strength. This implies that the yield strength is also independent of the interface between insert and cast matrix. The role of the insert for the elastic deformability is not well understood yet. This is a field of interest for further research.

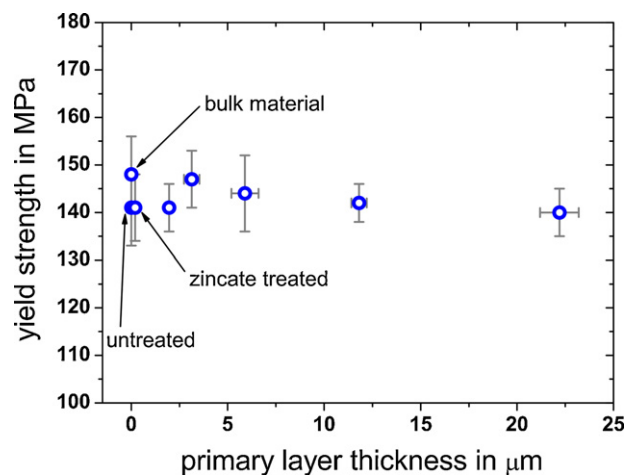


Fig. 11. Yield strength of the compound for different initial layer thicknesses.

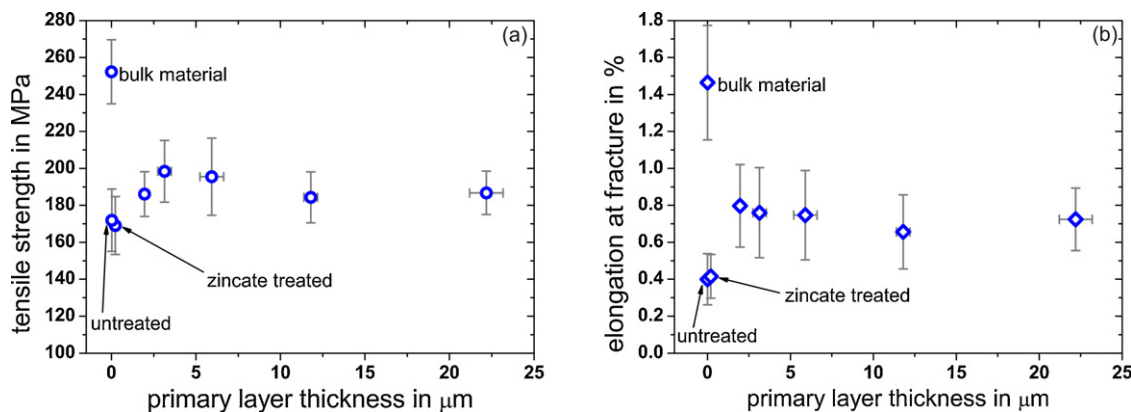


Fig. 12. Results of the tensile tests for different initial layer thicknesses: (a) tensile strength and (b) elongation at fracture.

The results of the plastic behaviour during the tensile test are shown in Fig. 12. Tensile strength and elongation at fracture are plotted against initial layer thickness. Basically, the results clarify that the insert is detrimental to these examined properties. Compared to the bulk material samples, the integration of the structure without additional pre-treatment lowers the tensile strength and the elongation at fracture about 30% and 75%, respectively. The zincate treatment of the structure without additional electrochemical deposition does not improve the plastic properties of the compound. The reason is the missing formation of a metallic bonding between the Al99.5 and the cast matrix. The additional electrodeposited Zn layer on the insert results in a slight increase of the tensile strength and a clear increase of the elongation at fracture. However, the tensile strength increase is within the range of the standard deviation. The enhancement of the plastic properties seems to be independent of the layer thickness. This means, width and composition of the transition zone have not much influence on the mechanical properties.

The plastic properties of the compound are determined by the insert's geometry, the formation of a metallic bonding and the material properties of the insert and the matrix. The volume fraction of the insert is just 0.1 of the compound. However, the influence of the geometry of the expanded metal, shown in Fig. 2, is a more important factor. Complex states of stress form inside the samples during plastic deformation of the compound. Hence, the real effect of the insert on the plastic properties of the compound is significantly higher than suggested by the volume fraction. Without a metallic bonding between insert and cast alloy the insert cannot contribute to the tensile strength as no stress can be transmitted. The continuous metallic transition enables stress transmission, but a significant enhancement of the material's strength with Al99.5 cannot be achieved. Considering the yield strength of Al99.5, the stress is relieved by plastic deformation. Therefore, the substitution of Al99.5 by a high-strength wrought alloy is a requirement for the fabrication of an aluminium–aluminium compound without loss of strength.

The increase of the elongation at fracture by creating a metallic bonding between the insert and the cast matrix can be explained by the suppression of the notch effect. The geometry of the expanded metal with the sharp edges results in many notches inside the compound. Without metallic bonding, the notches produce a three

dimensional state of tensile stress restricting the plastic deformability.

4. Conclusions

The fabrication of an aluminium–aluminium compound was successfully realised by high pressure die casting. A permanent activation of an Al insert's surface was achieved by combining zincate treatment and zinc galvanizing. The layer reacts during the casting process and a continuous metallic transition forms. Width as well as microstructure of the transition zone between matrix and insert varies with varying initial layer thickness.

The plastic properties of the compound are primarily dependent on the insert's material. Al99.5 can only partially compensate the reduction of the cast matrix volume as the yield strength is too small. A high-strength wrought alloy has to be used for the compound if an enforcement of the tensile strength is intended.

Acknowledgement

The underlying research is gratefully supported by the German Research Foundation (DFG) as part of the special research field SFB/TR 39.

References

- [1] V. Bräutigam, C. Körner, R.F. Singer, Patent specification DE 10 2005 016 402 B4 (2010).
- [2] M. Rübner, C. Körner, R.F. Singer, *Adv. Sci. Technol.* 56 (2008) 170–175.
- [3] W. Fragner, K. Papis, P. Uggowitzer, J. Wosik, *Giesserei-Praxis* 7–8 (2008) 243–248.
- [4] K.J.M. Papis, B. Hallstedt, J.F. Löffler, P.J. Uggowitzer, *Acta Mater.* 56 (2008) 3036–3043.
- [5] K.J.M. Papis, J.F. Loeffler, P.J. Uggowitzer, *Sci. China Ser. E* 52 (2009) 46–51.
- [6] Y. Boonyongmaneerat, C.A. Schuh, D.C. Dunand, *Scr. Mater.* 59 (2008) 336–339.
- [7] S. Wernick, R. Pinner, P.G. Sheasby, *The Surface Treatment and Finishing of Aluminium and its Alloys*, fifth ed., ASM International, Materials Park, OH, 1996.
- [8] X.P. Niu, B.H. Hu, I. Pinwill, H. Li, J. Mater. Process. Technol. 105 (2000) 119–127.
- [9] M.H.G. Jacobs, P.J. Spencer, *J. Alloys Compd.* 220 (1995) 15–18.
- [10] T.B. Massalski, H. Okamoto, P.R. Subramanian, L. Kacprzak, *Binary Alloy Phase Diagrams*, 2nd ed., ASM International, Materials Park, OH, 2001.
- [11] O. Saray, G. Purcek, *J. Mater. Process. Technol.* 209 (2009) 2488–2498.
- [12] M. Tavosi, M.H. Enayati, F. Karimzadeh, *J. Alloys Compd.* 464 (2008) 107–110.
- [13] A.A. Mazilkin, B.B. Straumal, E. Rabkin, B. Baretzky, S. Enders, S.G. Protasova, O.A. Kogtenkova, R.Z. Valiev, *Acta Mater.* 54 (2006) 3933–3939.